Ultra High Temperature High-Entropy Borides:

Effect of Graphite Addition on Oxides Removal and Densification Behaviour

Simone Barbarossa[1], Roberto Orrù[1, *], Sebastiano Garroni[2,3], Roberta Licheri[1], and Giacomo Cao[1]

[1]*Dipartimento di Ingegneria Meccanica, Chimica, e dei Materiali, Unità di Ricerca del Consorzio Interuniversitario Nazionale per la Scienza e Tecnologia dei Materiali (INSTM), Università degli Studi di Cagliari, via Marengo 2, 09123 Cagliari, Italy*

[2]*Dipartimento di Chimica e Farmacia, Università degli Studi di Sassari, Via Vienna 2, 07100 Sassari, Italy*

[3]*International Research Centre in Critical Raw Materials-ICCRAM, University of Burgos, Plaza Misael Bañuelos s/n, 09001 Burgos, Spain*

[*]Corresponding author: Roberto Orrù - roberto.orru@dimcm.unica.it

https://doi.org/10.1016/j.ceramint.2020.10.200

Abstract

The introduction of 0.5-1.0 wt.% graphite to the powders prepared by Self-propagating High-temperature Synthesis (SHS) is found to be highly beneficial for the removal of oxide impurities (from 2.7-8.8 wt.% to 0.2-0.5 wt.%) during spark plasma sintering (1950°C/20 min, 20 MPa) of $(Hf_{0.2}Mo_{0.2}Ta_{0.2}Nb_{0.2}Ti_{0.2})B_2$ and $(Hf_{0.2}Mo_{0.2}Ta_{0.2}Zr_{0.2}Ti_{0.2})B_2$ ceramics. Concurrently, the consolidation level achieved is enhanced from about 92.5% and 88%, respectively, to values exceeding 97%. While a further increase of graphite slightly improves samples densification, final products become progressively richer of the unreacted carbon.

It is assumed that graphite plays a double role during SPS, e.g. not only as a reactant during the carbothermal reduction of oxides contaminant, but also as lubricating agent for the powder particles. The latter phenomenon is likely the main responsible for the densification improvement when 3 wt.% or larger amounts of additive are used. Another positive effect is the crystallite size refinement of the high-entropy phases with the progressive abatement of oxides, to confirm that their presence promotes grain coarsening during the sintering process.

Keywords: High-entropy metal borides; Oxide impurities; Spark Plasma Sintering; Self-propagating High-temperature Synthesis; X-ray diffraction.

1. Introduction

After its recent discovery, the emerging class of ultra-high temperature ceramics (UHTCs) known as High Entropy Borides (HEBs) has immediately attracted a significant attention by the scientific community, due their potential applications in several fields **[1-14]**.

In HEBs, transition metal cations are uniformly distributed in near-equimolar proportion into the diboride lattice, to provide thermodynamically stable single-phase crystalline solid solutions with maximum configurational entropy **[15]**.

Different research groups around the world have conducted several investigations in the last years aimed to synthesize and characterize diverse members of these refractory materials **[2-14]**. While only few studies were specifically focused on the synthesis of HEBs in powder form **[5,10,12]** or films **[2]**, the other investigations were aimed to the fabrication of bulk bodies **[1,3,4,6-9,11,13,14]**. It should be noted that Spark Plasma Sintering (SPS) is undoubtedly the preferred technique employed to produce dense HEBs **[1,3,4,6-8,11,13,14,16].** Alternatively, SPS was also recently used for the preparation of pre-sintered samples to be subsequently processed by induction heating **[9]**. Such wider utilization of this technique is readily justified by the more convenient processing conditions generally required with respect to conventional hot-pressing methods **[17]**.

When using SPS, sintering temperatures in the range 1950-2050°C are typically adopted to achieve high relative densities **[3,7,8,11]** and/or good compositional uniformity **[1,4,6,11,13]** in the end products.

SPS is usually preceded by an additional processing step, which is aimed to the synthesis of high-entropy boride powders or to the activation of the related precursors **[1,3,4,6,8,9,11,13,14]**.Indeed, the only attempt made so far to prepare dense single-phase HEBs in one-step from non-pretreated elemental powders, according to the so called Reactive SPS, did not succeed **[13]**.

Unfortunately, oxides and/or other contaminants are often detected in the obtained bulk materials **[1,3,7,8]**. Such impurities are either originally present in the raw powders or formed during the fabrication

process. For instance, residual oxides are found in SPS ceramics obtained from powders synthesized via borothermal or boro-carbothermal reduction **[3,7,8]** Similarly, the relatively long duration (6h) of the high energy Ball Milling (BM) process preceding the SPS stage in **Gild et al. [1]** is responsible for the formation of such undesired phases. A shorter BM treatment (5-60 min) was also considered to process the powders prepared by Self-propagating High temperature Synthesis (SHS) and used for the obtainment of massive $(Hf_{0.2}Zr_{0.2}Ta_{0.2}Nb_{0.2}Ti_{0.2})B_2$ by SPS **[6,13]**. In this regard, oxygen contamination during BM is also the plausible reason for justifying that no densification improvement was observed when the mechanical treatment was prolonged from 20 to 60 min **[13]**.

Oxides impurities in MeB_2 (Me= transition metal) are often associated to MeO_2 and B_2O_3 **[18-21]**, although different O-containing phases, for instance amorphous Zr-B-C-O, were also detected on the surface of ZrB_2 powders **[22]**.

Regardless of their origin and form, O-contamination in metal borides is known to be detrimental for their consolidation **[18-20,22-24]**. Indeed, when such impurities are present, grain coarsening is accelerated, due to the evaporation–condensation mechanism, so that the driving force for densification is consequently lowered [**18-20]**

The use of certain additives, such as carbon **[3,19,20,23],** B_4C **[19]**, or TiC **[20]**, was suggested to overcome this drawback.

In this work, the presence of oxides impurities in sintered $(Hf_{0.2}Mo_{0.2}Ta_{0.2}Nb_{0.2}Ti_{0.2})B_2$ ceramics obtained from 60 min ball milled SHS powders is first proven. Subsequently, the effect produced on the densification and composition of SPS samples when adding different amounts of graphite (0-10 wt.%) to the SHS powders is systematically investigated. The proposed approach is also validated with another high entropy boride system, i.e. $(Hf_{0.2}Mo_{0.2}Ta_{0.2}Zr_{0.2}Ti_{0.2})B_2$, fabricated for the first time according to the SHS-SPS processing route. It should be mentioned that the two compositions considered in this work

correspond to bulk ceramics which are shown to possess, compared to alternative HEBs, rather high hardness and oxidation resistance properties **[1, 11]**.

To the best of our knowledge, the quantitative evaluation of the amount and crystallite size of high-entropy and other phases present in the sintered products, as a function of the graphite added to the SHS powders, is performed for the first time in the literature.

2. Materials and methods

Commercially available Hf (Alfa Aesar, cod. 00337, particle size < 44 μm, 99.6 % purity), Mo (Aldrich, cod 266892, particle size < 149 μm, ≥ 99% purity), Ta (Alfa Aesar, cod 00337, particle size < 44 μm, 99.9 % purity), Nb (Alfa Aesar, cod 010275, particle size < 44 μm, 99.8 % purity), Ti (Aldrich, cod 268496, particle size < 149 μm, 99.7 purity), Zr (Alfa Aesar, cod 00418, particle size < 44 μm, > 98.5 % purity), B (Aldrich, cod 15580, amorphous, ≥ 99 % purity), and graphite (Aldrich, cod 282863, particle size < 20 μm) powders were used in the present study. The two starting mixtures to be reacted by SHS for the preparation of $(Hf_{0.2}Mo_{0.2}Ta_{0.2}Nb_{0.2}Ti_{0.2})B_2$ and $(Hf_{0.2}Mo_{0.2}Ta_{0.2}Nb_{0.2}Ti_{0.2})B_2$, respectively, were prepared by mixing reactants for 20 min in a SPEX 8000 (SPEX CertiPrep, USA) shaker mill using plastic vials and alumina balls, according to the following reactions:

$$0.2Hf+0.2Mo+0.2Ta+0.2Nb+0.2Ti + 2.2B \rightarrow (Hf_{0.2}Mo_{0.2}Ta_{0.2}Nb_{0.2}Ti_{0.2})B_2 \quad (1)$$

$$0.2Hf+0.2Mo+0.2Ta+0.2Zr+0.2Ti + 2.2B \rightarrow (Hf_{0.2}Mo_{0.2}Ta_{0.2}Zr_{0.2}Ti_{0.2})B_2 \quad (2)$$

The 10 mol.% excess of Boron, with respect to the stoichiometric value needed for the synthesis of metal diborides, is used to compensate its partial loss during reaction evolution, as reported elsewhere **[25-27]**. In particular, the boron/metal atomic ratio considered in Eq. (1)-(2) was found to be the optimal value to maximize the conversion degree of initial reactants to the desired HEB phase **[13]**.

SHS reactions were carried out on cylindrical pellets obtained by uniaxially pressing the reactants mixture. Once locally activated by an electrically heated tungsten coil, the synthesis process took place very rapidly (few seconds) inside a stainless-steel chamber filled with Argon. Details on the related experimental set-up and procedure can be found in a previous work **[28]**.

The SHS made product was first hand crushed in a mortar, then mixed with different amounts of graphite (0, 0.5, 1.0, 3.0, and 10.0 wt.%) and the resulting powders were mechanically treated for 60 min (ball to powder ratio equal to 2) using a SPEX 8000 (SPEX CertiPrep, USA) device with stainless steel

vial and four steel balls (10 mm diameter, about 4.5 g weight). No contamination from milling tools was detected under such conditions.

All mixtures were processed for 20 min at 1950°C (20 MPa applied pressure and about 200 °C/min heating rate) by SPS using a 515S model apparatus (Fuji Electronic Industrial Co., Ltd., Kanagawa, Japan) operating under vacuum conditions (about 20 Pa). The sintering process was conducted under temperature-controlled mode using an infrared pyrometer (CHINO, mod. IR-AHS2, Japan) focused on the lateral surface of the cylindrical die (30 mm external diameter; 15 mm inside diameter; 30 mm height). The latter one and the related two plungers (14.7 mm diameter, 20 mm height) consisted of AT101 graphite supplied by ATAL Srl. (Italy). To make sample release easier at the end of the SPS process, the internal surfaces of the die and the top and bottom surface of the plungers were lined with graphite foils (99.8 % pure, 0.13 mm thick, Alfa Aesar, Karlsruhe, Germany). With the aim of minimizing heat losses by radiation, the die was externally covered with a layer of graphite felt. The displacement data recorded during the SPS process were properly corrected by subtracting the thermal expansion contribution and obtaining the sample shrinkage curves.

Disks of about 14.7 mm diameter and 3 mm thickness were finally produced. For the sake of reproducibility, each experiment was repeated at least twice.

The absolute density of polished samples was measured using the Archimedes' method and distilled water as immersion medium. To determine relative densities, the theoretical values of 8.67 and 8.52 g/cm^3 for $(Hf_{0.2}Mo_{0.2}Ta_{0.2}Nb_{0.2}Ti_{0.2})B_2$ and $(Hf_{0.2}Mo_{0.2}Ta_{0.2}Zr_{0.2}Ti_{0.2})B_2$, respectively, were considered **[1]**. In addition, the theoretical densities of the systems obtained with graphite were calculated through a rule of mixture **[29]**. In this regard, the density value of 2.26 g/cm^3 was used for graphite **[30]**, and the calculation was carried out by considering the weight content of this additive initially introduced in the mixture. The validity of latter assumption will be verified in the Results section.

Phase analysis was performed by X-ray diffraction (Philips PW 1830, Netherlands) using Cu K_α radiation, over a range of scattering angles 2ϑ from 20° to 130°, in steps of 0.05° with 15 s acquisition time per angle. The Rietveld method was employed to determine phases amount (wt.%) and the related structural parameters by analyzing the XRD patterns with the MAUD program **[31]**.

Products microstructure and composition were also analyzed by high resolution scanning electron microscopy (HRSEM) (mod. S4000, Hitachi, Tokyo, Japan) equipped with a UltraDry EDS Detector (Thermo Fisher Scientific, Waltham, MA, USA). SEM images were processed with the open source software ImageJ (version 1.54a for Windows, 64 bit, National Institutes of Health, Bethesda, MD, USA) **[32]** to quantify residual porosity in SPS samples.

3. Results

3.1. The ($Hf_{0.2}Mo_{0.2}Ta_{0.2}Nb_{0.2}Ti_{0.2}$)$B_2$ system

The results relative to the synthesis of ($Hf_{0.2}Mo_{0.2}Ta_{0.2}Nb_{0.2}Ti_{0.2}$)$B_2$ by SHS according to Eq. (1), as well as the characteristics of the obtained powders, can be found elsewhere **[13]**.

Figure 1 shows, on a log scale, the XRD experimental patterns (red rhombohedral) and the best fit relative to the ($Hf_{0.2}Mo_{0.2}Ta_{0.2}Nb_{0.2}Ti_{0.2}$)$B_2$ products obtained by SPS using SHS powders to which different amounts of graphite were added. As for the additive-free sintered samples, this analysis evidences both the main HEB phase and the presence of small peaks ascribed to monoclinic and cubic HfO_2. The total content of these oxides, estimated by the Rietveld procedure, was about 2.7 wt.%. As seen in **Figure 1**, the oxide peaks tend to progressively disappear with the use of graphite. However, they are found again in the pattern of the SPS product obtained for the case of 10 wt.% C. No carbide phases were detected by this analysis.

The effect produced by the introduction of graphite on phase quantity is shown in **Figure 2(a)**. The numerical values of all the parameters estimated by the fit analysis can be found in Supplementary **Table S1**. These data evidence that the introduction of 0.5 and 1 wt.% of additive is accompanied by a marked decrease of the total amount of HfO_2, i.e. 0.7 and 0.2 wt.%, respectively. Correspondingly, the relative content of the HEB phase in the sintered products increases, and so does residual graphite, as shown in **Figure 2(a)** and **Table S1**. While no further decrease in the oxide content is observed when the graphite addition was augmented to 3 wt.%, a significantly higher content of HfO_2 (2.1 wt.%) was detected with 10 wt.% C. **Figure 2(a)** and **Table S1** also indicate that residual graphite in the SPS product is only slightly lower than that initially added to the SHS powders. **Figure 2(b)** shows the evolution of crystallite size of the ($Hf_{0.2}Mo_{0.2}Ta_{0.2}Nb_{0.2}Ti_{0.2}$)$B_2$ phase in the SPS product as a function of the graphite fraction. It is seen that this parameter decreases significantly with the introduction of 0.5 wt.% C, i.e. from approximately

1200 to 800 Å (mean values). The latter value remains approximately constant up to 3 wt.% C whereas it raises again to about 1300 Å when 10 wt.% graphite is employed.

The influence of graphite addition on the density of sintered samples can be deduced from **Figure 3**. Progressively higher absolute density values are obtained with graphite percentages up to 1 wt.%. On the other hand, the measured density decreases when the amount of additive is augmented. However, if all these data are referred to the theoretical densities, the resulting relative values increase in the compositional range 0.0-3.0 wt.% C, whereas negligible changes are observed when the additive content was augmented to 10.0 wt.%. The major effect is attained in the 0.0-1.0 wt.% interval, where the densification level increases from 92.5% to values above 97%, respectively. As graphite is further augmented, product consolidation slightly improves to values of about 98%.

The SEM micrographs and related EDS maps of SPS products obtained with different graphite quantities are reported in **Figure 4**. All specimens display a good compositional homogeneity, while powder densification gradually improves with graphite. In particular, the residual porosities estimated by image analysis for 0, 0.5 and 1.0 wt.% C are 6.8±0.3, 5.7±0.6, and 1.2±0.2 vol.%, respectively. Finally, porosity values down to 1 vol.% are obtained for 3.0 and 10.0 wt.% of graphite.

EDS analysis did not evidence the presence of regions, locally rich in carbon, in samples produced with 1.0 wt.% or lower amounts of graphite. On the other hand, unreacted carbon is clearly detected in materials sintered after adding 3.0 and, above all, 10.0 wt.% C to the SHS powders. It should be noted that, the highly irregular surface of the sample with 10 wt.% C **(Figure 4e)**, which corresponds to approximately 30 vol.% C in the composite ceramic, is ascribed to the fact that part of the residual graphite was pulled-out during sample preparation for metallography. This holds also true, albeit at a much lower degree, for 3.0 wt.% C. In addition, since the amount of oxides was too small in all the produced samples, as revealed by the Rietveld method, their presence could not be evidenced by EDS analysis.

3.2. The $(Hf_{0.2}Mo_{0.2}Ta_{0.2}Zr_{0.2}Ti_{0.2})B_2$ system

The XRD pattern of the powders obtained after the SHS reaction (2) is compared in **Figure 5** with that of the starting reactants mixture. Boron was not revealed by this analysis due to its amorphous character. The synthesis process did not go to completion while a multiphase product is finally obtained. As indicated by the Rietveld analysis, whose results are reported in **Table S2** of the Supplementary material, the synthesized ceramic consisted for almost 70 wt.% of the desired HEB phase. The secondary boride phases also found include $(Hf_{0.5}Ti_{0.5})B_2$, $(ZrTiB_4)_{0.5}$, TaB_2, and HfB_2, whose content was estimated to be equal to 13.7, 11.3, 5.6, and 0.9 wt.%, respectively. Traces (not quantified) of unreacted Mo and other minor phases are also detected.

As for the other HEB system described in section **3.1.**, different mass fractions of graphite (0.5, 1.0 and 3.0 wt.%) were added to these powders before their consolidation. In contrast, since the introduction of 10.0 wt.% C did not provide beneficial effects to the characteristics of sintered $(Hf_{0.2}Mo_{0.2}Ta_{0.2}Nb_{0.2}Ti_{0.2})B_2$ samples, such condition was not investigated when considering the case of the $(Hf_{0.2}Mo_{0.2}Ta_{0.2}Zr_{0.2}Ti_{0.2})B_2$ ceramic.

The effect produced by graphite addition on the composition of the SPS samples can be deduced from the related XRD patterns shown in **Figure 6.** The presence of oxide peaks in the additive-free product, along with those corresponding to the main high-entropy phase, is evident. As estimated by the Rietveld analysis (**Table S3**), the oxides content was approximately 8.8 wt.%. The intensities of HfO_2 peaks decrease as the amount of graphite was augmented. The compositional changes, in terms of mass fractions of the different phases, and the average crystallite size of the $(Hf_{0.2}Mo_{0.2}Ta_{0.2}Zr_{0.2}Ti_{0.2})B_2$ phase, are plotted in **Figure 7a-7b**, respectively. Further details can be found in **Table S3** of the Supplementary material. **Figure 7a** indicates that oxide content drastically decreases to 2.0 and 0.5 wt.% with the addition of 0.5 and 1.0 wt.% C, respectively. No further changes are observed with 3.0 wt.% C, except for the unreacted graphite remained in the sintered material, which is responsible for the corresponding reduction

of the HEB mass fraction. Also in this case, according to the XRD analysis, no carbide phases were formed during the sintering process. Furthermore, data reported in Supplementary **Tables S1** and **S3** indicate that the content of residual graphite in bulk products is only slightly lower than that initially present in the powder mixture to be processed by SPS. This demonstrates that only a small amount of carbon is consumed by carbothermal reactions. Consequently, the assumption made to calculate the theoretical densities of the various composite systems, i.e. by considering the initial additive percentage, is quite reasonable.

As the amount of graphite was augmented, the graph reported in **Figure 7b** shows a monotonical reduction, with a progressively decreasing rate, of the average crystallite size of the $(Hf_{0.2}Mo_{0.2}Ta_{0.2}Zr_{0.2}Ti_{0.2})B_2$ phase. In particular, the estimated value of this parameter changed from about 1200 to 700 Å, as a result of the introduction of 1.0 wt. % of additive.

The plot of the measured density as a function of the graphite added to the powders is shown in **Figure 8**, along with the corresponding theoretical and relative values. As for the $(Hf_{0.2}Mo_{0.2}Ta_{0.2}Nb_{0.2}Ti_{0.2})B_2$ system, the maximum absolute density is reached with 1.0 wt.% C. Nonetheless, the corresponding relative density curve displays a continuous increasing trend in the entire compositional range. Specifically, only 87% dense samples are obtained with no additive, while average relative densities of about 97 and 99% are achieved with 1.0 and 3.0 wt.% of graphite, respectively.

The densification behavior of these groups of powders can be seen in **Figure 9**, where the sample shrinkage curves of mixtures with diverse amounts of graphite (0.0, 1.0 and 3.0 wt.%) are plotted along with the prescribed temperature profile. Since the beginning of the SPS process, higher shrinkage values are measured with powder compacts containing graphite. However, such differences become more significant after about 9 min from the beginning of the current application, when the measured temperature was below 1800°C. Correspondingly, both the 1.0 and 3.0 wt.% C mixtures display a markedly higher consolidation ability with respect to the additive-free powders.

A SEM micrograph and the related elemental EDS maps of the sample obtained with no graphite are compared in **Figure 10a-10b** with those relative to the specimen produced with 1.0 wt.% C under the same SPS conditions. Albeit a uniform composition is evidenced by EDS analysis in the graphite-free ceramic (**Figure 10a**), the latter one also exhibits a high residual porosity, consistently with the measured density value reported in **Figure 8**. Based on image analysis, a residual porosity of 9.1 ± 0.8 vol.% is present in this specimen. In contrast, **Figure 10b** indicates that the introduction of graphite determines a clear improvement in product densification along with a very good elemental distribution across the sample. The porosity level obtained in this case was 2.2 ± 0.2 vol.%.

4. Discussion

Differently from the case of individual transition metal borides, which were successfully synthesized by SHS from their elements with no secondary phases **[26,27,33,34]**, the results reported in the present and previous works **[6,13]** indicate that this goal is far from being reached by this technique when considering the high-entropy $(Hf_{0.2}Mo_{0.2}Ta_{0.2}Nb_{0.2}Ti_{0.2})B_2$ and $(Hf_{0.2}Mo_{0.2}Ta_{0.2}Zr_{0.2}Ti_{0.2})B_2$ products.

This outcome could be likely explained by the peculiar features of the SHS process **[35]**, which evolves so rapidly, quite far from the equilibrium conditions, that the six different elements comprised in each of these HEB systems are not able to be suitably combined for generating such a complex single-phase material. In contrast, relatively longer treatments at high-temperatures must be applied to speed-up diffusion and other physico-chemical phenomena involved in the synthesis process. Despite it, the SHS technique has been proven to be very efficient and fast to provide multiphase products, mostly consisting of the desired HEB phase (70 wt.% or higher amounts), where a good mixing level between the different elements is achieved.

Such outcome is found to highly promote the formation of single phase $(Hf_{0.2}Mo_{0.2}Ta_{0.2}Nb_{0.2}Ti_{0.2})B_2$ and $(Hf_{0.2}Mo_{0.2}Ta_{0.2}Zr_{0.2}Ti_{0.2})B_2$ during the subsequent SPS treatment at 1950°C (20 min, 20 MPa). In this regard, as mentioned in the Introduction, the consolidation of 20 min milled SHS powders was found to guarantee the latter achievement, with no oxides detected in the sintered ceramic **[6]**. However, the product density was only 92.5%, while the attempt made to improve it with the extension of the milling time to 60 min, did not provide the expected beneficial effects **[13]**.

The further analysis conducted in the present work evidenced that the sintered $(Hf_{0.2}Mo_{0.2}Ta_{0.2}Nb_{0.2}Ti_{0.2})B_2$ material obtained under the latter conditions contained about 2.7 wt.% oxides. The presence of even larger amounts of oxides (up to 8.8 wt.%) is also found in $(Hf_{0.2}Mo_{0.2}Ta_{0.2}Zr_{0.2}Ti_{0.2})B_2$ product prepared according to the same processing route. In addition, the relative density of the corresponding sintered samples was very low, i.e. about 87% (**Figure 8**).

Since no contaminants were detected in the material obtained after 20 min BM **[6]**, this drawback could be necessarily attributed to the prolonged mechanical treatment (60 min). This agrees with the literature, since it is well recognized that ball milling of non-oxide ceramics typically leads to oxygen contamination **[1,21,22,24]**. Nonetheless, such impurities were also found in sintered products obtained from powders prepared by borothermal and boro-carbothermal reduction **[7,8]**

Irrespective of the reason for the presence of O impurities in HEBs, their elimination/reduction represents a crucial issue for achieving high consolidation levels by SPS. The results obtained in the present work unequivocally testify that the introduction of small amounts of graphite (0.5 and 1 wt.%) to the SHS powders is enough to provide beneficial effects in terms of oxides removal and products consolidation. In particular, the optimal condition for minimizing HfO_2 contaminants and concurrently achieving relative density values above 97% for both $(Hf_{0.2}Mo_{0.2}Ta_{0.2}Nb_{0.2}Ti_{0.2})B_2$ and $(Hf_{0.2}Mo_{0.2}Ta_{0.2}Zr_{0.2}Ti_{0.2})B_2$ sintered products is 1.0 wt.% C. On the other hand, while a further improvement in materials density was produced with an increase of the additive to 3 wt.%, a relatively large amount of residual graphite (2.6-2.8 wt.%) was found in the resulting ceramics. Moreover, no further decrease in oxides content was obtained. Surprisingly, when the case of 10 wt.% C was investigated for the $(Hf_{0.2}Mo_{0.2}Ta_{0.2}Nb_{0.2}Ti_{0.2})B_2$ system, the quantity of oxide contaminants in the SPS product was comparable even to that observed in samples with no graphite. This aspect will be discussed later.

Let's now examine the role played by graphite during the SPS process. Firstly, such additive clearly acts as a reactant in the carbothermal reduction of oxides, which is likely the primary motivation for the decrease of these impurities and the simultaneous improvement of powder consolidation observed for the cases of 0.5 and 1.0 wt.% C. On the other hand, when larger amounts of graphite are used, the relative density of the sintering product increases with no additional beneficial effects in terms of oxides removal.

In this regard, to justify the enhanced densification observed during SPS when 2 wt.% of graphite was added to ZrB_2 powder, **Zamora et al. [21]** postulated the lubricating action of this additive rather than the

carbothermal reduction of oxides. The fact that oxides were still present in the sintered product, while graphite was found dispersed in the sintered ceramic, supported such explanation. As described above, a different situation was observed in our study when considering 0.5 or 1 wt.% C. On the other hand, similar outcomes to those described by **Zamora et al. [21]** are encountered in the present work, when the additive amount was further increased (3.0 and, above all, 10.0 wt. %). Therefore, under the latter conditions, graphite probably plays a key role as lubricating agent, thus inducing the improvement of powder densification.

The effect produced by the addition of amorphous C in the range 0.0-10.0 wt.% on the sintering behavior of ZrB_2 powders synthesized by SHS was systematically investigated by **Mishra and Pathak [20]**. The observed densification improvement with an increase of C content from 0.0 to 4.0 wt.% was associated to oxides removal on the particles surface, which consequently makes them more active. On the other hand, the use of C in the range 4.0-10 wt.% was found to hinder powder consolidation. In contrast with the latter result, only modest changes in product density are observed in our study in the range 3.0-10.0 wt.% C (**Figure 3**). This could be likely explained with the fact that the amorphous C used by **Mishra and Pathak [20]** is not able to provide the lubricating action observed with graphite. In addition, the use of the SPS technique instead of pressureless sintering could also explain such discrepancy.

Another interesting finding is the change of crystallite size of the HEB phase as graphite is progressively introduced in the powder mixture (**Figures 2b** and **7b)**. A pronounced product refinement is obtained when relatively small amounts of the additive are utilized (0.5-1 wt.%), while no or minor changes are observed up to 3 wt.%. In contrast, the opposite outcome is seen when graphite was increased from 3 to 10 wt.% (**Figure 2a**). In this context, it is important to note that the curves reporting the oxide content (**Figures 2a** and **7a)** and the corresponding crystallite size (**Figures 2b** and **7b)** follow similar trends, for both HEB systems. In addition, the estimated average crystallite dimension in additive-free

$(Hf_{0.2}Mo_{0.2}Ta_{0.2}Nb_{0.2}Ti_{0.2})B_2$ samples resulting from 20 min BM powders, where no oxides impurities were detected by XRD, was relatively smaller (869 Å) **[6]** in comparison with that obtained in this work. All these outcomes are consistent with the fact that the presence of oxides promotes grain coarsening during the SPS process. This is also in agreement with the grain growth inhibition observed by **Mishra and Pathak [20]** with the addition of C to ZrB_2 powders.

The systematic investigation conducted in this work allowed us to identify the most convenient graphite quantity, i.e. 1.0 wt.%, to be added to the SHS powders to guarantee the obtainment by SPS of highly dense and homogeneous $(Hf_{0.2}Mo_{0.2}Ta_{0.2}Nb_{0.2}Ti_{0.2})B_2$ and $(Hf_{0.2}Mo_{0.2}Ta_{0.2}Nb_{0.2}Ti_{0.2})B_2$ ceramics, basically consisting of the desired phases only. Indeed, the use of higher additive amounts leads to significant amounts of residual graphite in the sintered product. In this regard, high densification levels (99.3 %) were recently achieved by **Gild et al. [3]** with the introduction of 3 wt.% graphite to a mixture of individual borides for the fabrication of $(Hf_{0.2}Zr_{0.2}Ta_{0.2}Nb_{0.2}Ti_{0.2})B_2$ by flash SPS. However, the XRD analysis indicated that small amount of a cubic carbide phase was also formed, whereas SEM investigation revealed the presence of residual graphite in the product.

It is worth noting that the presence of graphite or carbide phases might not be desirable for certain high temperature applications, particularly when operating under harsh oxidizing environments. Therefore, in these circumstances, the content of such phases should be minimized. To this aim, the results obtained in this work clearly indicate that, at least when taking advantage of the SHS-SPS method, very small amounts of graphite (1.0 wt.% at most) are sufficient to strongly remove oxides contaminant and simultaneously improve product density, while avoiding or significantly limiting the presence of residual carbon in sintered HEBs.

4. Conclusions

Based on the results obtained in this work, focused on the fabrication of high entropy $(Hf_{0.2}Mo_{0.2}Ta_{0.2}Nb_{0.2}Ti_{0.2})B_2$ and $(Hf_{0.2}Mo_{0.2}Ta_{0.2}Zr_{0.2}Ti_{0.2})B_2$ ceramics by SPS (1950°C/20 min/20 MPa) using 60 min ball milled SHS powders with different amounts of graphite, it is possible to draw the following main conclusions.

1) Relatively low dense samples, up to 92.5 and 88 %, respectively, consisting of the desired high entropy phases with 2.7 and 8.8 wt.% oxide impurities, respectively, are obtained when no graphite was added to the SHS powders.
2) The introduction of small amounts of graphite (0.5-1.0 wt.%) markedly purifies the material, with a significant reduction of the oxide content (down to 0.2 and 0.5 wt.%, respectively); simultaneously, an enhancement of powder consolidation is attained, with relative densities exceeding 97 % of their theoretical values.
3) As the graphite amount is further augmented, the consolidation level is still improved (above 98 and 99%) while no additional benefits are obtained regarding oxides removal. In addition, under such conditions, most of the graphite added to the SHS powder is included in the microstructure of the SPS product.
4) The optimal amount of graphite needed to minimize oxide impurities for the fabrication of dense $(Hf_{0.2}Mo_{0.2}Ta_{0.2}Nb_{0.2}Ti_{0.2})B_2$ and $(Hf_{0.2}Mo_{0.2}Ta_{0.2}Zr_{0.2}Ti_{0.2})B_2$ is 1.0 wt.%.
5) A crystallite size refinement is observed as oxides are progressively removed, to indicate that the presence of the latter ones accelerates grain coarsening during the sintering process.
6) It is reasonable that graphite plays a double role in the improvement of powder densification, i.e. as a reactant in the carbothermal reduction of oxides as well as a lubricating agent. The first contribution is likely more significant when relatively small amounts of additive are used, i.e. 0.5-1.0 wt.% C, since a marked oxides removal is correspondingly obtained. On the other hand, the

lubrication action of graphite becomes more relevant when larger amounts of this additive are utilized.

The approach adopted in the present work, based on the use of the SHS-SPS route with the beneficial contribution of small amounts of graphite as additive, is intended to be valid also for the fabrication of other high-entropy non oxides ceramics in bulk form.

Acknowledgements

The present work has been carried out in the framework of the ARCHIMEDES project sponsored by Regione Autonoma della Sardegna (Italy) - Fondo di Sviluppo e Coesione (FSC) 2014-2020 (Cod. RAS: RASSR88309, Cod. CUP: F76C18000980002). One of the authors (S.B.) performed his activity in the framework of the International PhD in Innovation Sciences and Technologies at the University of Cagliari, Italy. One of us (G.C.) acknowledges the results obtained in this manuscript as quite important for the "Ithermal" and "Generazione E" projects, sponsored by Sardegna Ricerche, Italy (Cod. CUP: F21I18000130006) and by the Italian Ministry of Education, University and Research, Italy (Cod. CUP: B96G18000560005), respectively. Thanks are due to Dr. Massimiliano Murgia (University of Cagliari) for his useful contribution as well as Mr. Daniele Lai and Mr. Gianluca Marongiu (University of Cagliari) for their technical assistance.

References

[1] J. Gild, Y. Zhang, T. Harrington, S. Jiang, T. Hu, M.C. Quinn, W.M. Mellor, N. Zhou, K. Vecchio, J. Luo, 2016. High-Entropy Metal Diborides: A New Class of High-Entropy Materials and a New Type of Ultrahigh Temperature Ceramics, Sci Rep. 6, 37946. https://doi.org/10.1038/srep37946

[2] P.H. Mayrhofer, A. Kirnbauer, P. Ertelthaler, C.M. Koller, High-entropy ceramic thin films; A case study on transition metal diborides, Scripta Mater. 149 (2018) 93-97. https://doi.org/10.1016/j.scriptamat.2018.02.008

[3] J. Gild, K. Kaufmann, K. Vecchio, J. Luo, Reactive flash spark plasma sintering of high-entropy ultrahigh temperature ceramics, Scripta Mater.170 (2019) 106-110. https://doi.org/10.1016/j.scriptamat.2019.05.039

[4] J.F. Gu, J. Zou, S.K. Sun, H. Wang, S.Y. Yu, J. Zhang, W. Wang, Z. Fu, Dense and pure high-entropy metal diboride ceramics sintered from self-synthesized powders via boro/carbothermal reduction approach, Sci China Mater. 62 (2019) 1898-1909. https://doi.org/10.1007/s40843-019-9469-4

[5] D. Liu, T. Wen, B. Ye, Y. Chu, Synthesis of superfine high-entropy metal diboride powders, Scripta Mater. 167 (2019) 110-114. https://doi.org/10.1016/j.scriptamat.2019.03.038

[6] G. Tallarita, R. Licheri, S. Garroni, R. Orrù, G. Cao, Novel processing route for the fabrication of bulk high-entropy metal diborides, Scripta Mater. 158 (2019) 100-104. https://doi.org/10.1016/j.scriptamat.2018.08.039

[7] Y. Zhang, W.-M., Guo, Z.-B. Jiang, Q.-Q. Zhu, S.-K. Sun, Y. You, K. Plucknett, H.-T. Lin, Dense high-entropy boride ceramics with ultra-high hardness, Scripta Mater. 164 (2019) 135-139. https://doi.org/10.1016/j.scriptamat.2019.01.021

[8] Y. Zhang, Z.-B. Jiang, S.-K. Sun, W.-M. Guo, Q.-S. Chen, J.-X. Qiu, K. Plucknett, H.-T. Lin, Microstructure and mechanical properties of high-entropy borides derived from boro/carbothermal

reduction, J. Eur. Ceram. Soc. 39(13) (2019) 3920-3924. https://doi.org/10.1016/j.jeurceramsoc.2019.05.017

[9] S. Failla, P. Galizia, S. Fu, S. Grasso, D. Sciti, Formation of high entropy metal diborides using arc-melting and combinatorial approach to study quinary and quaternary solid solutions, J Eur Ceram Soc. 40(2020) 588-593. https://doi.org/10.1016/j.jeurceramsoc.2019.10.051

[10] L. Feng, W.G. Farenholtz, G.E. Hilmas, Two-step Synthesis process for high-entropy diboride powders, J. Am. Ceram. Soc. 103(2020) 724-730. https://doi.org/10.1111/jace.16801

[11] J. Gild, A. Wright, K. Quiambao-Tomko, M. Qin, J.A. Tomko, Md Shafkat bin Hoque, J.L. Braun, B. Bloomfield, D. Martinez, T. Harrington, K. Vecchio, P.E. Hopkins, J. Luo, Thermal conductivity and hardness of three single-phase high-entropy metal diborides fabricated by borocarbothermal reduction and spark plasma sintering, Ceram Int. 46 (2020) 6906-6913. https://doi.org/10.1016/j.ceramint.2019.11.186

[12] F. Monteverde, F. Saraga, 2020. Entropy stabilized single-phase (Hf,Nb,Ta,Ti,Zr)B_2 solid solution powders obtained via carbo/boro-thermal reduction, J. Alloys Compd. 824, 153930. https://doi.org/10.1016/j.jallcom.2020.153930

[13] G. Tallarita, R. Licheri, S. Garroni, S. Barbarossa, R. Orrù, G. Cao, High-entropy transition metal diborides by reactive and non-reactive spark plasma sintering: A comparative investigation, J Eur Ceram Soc.40 (2020) 942-952. https://doi.org/10.1016/j.jeurceramsoc.2019.10.031

[14] Y. Zhang, S.K. Sun, W. Zhang, Y. You, W.M. Guo, Z.W. Chen, J.H. Yuan, HT. Lin, Improved densification and hardness of high-entropy diboride ceramics from fine powders synthesized via borothermal reduction process, Ceram. Int. 46 (2020) 14299-14303. https://doi.org/10.1016/j.ceramint.2020.02.214

[15] A.J. Wright, J. Luo, A step forward from high-entropy ceramics to compositionally complex ceramics: a new perspective, J. Mater. Sci. 55 (2020) 9812–9827. https://doi.org/10.1007/s10853-020-04583-w

[16] X.Q. Shen, J.X. Liu, F. Li, G.J. Zhang, Preparation and characterization of diboride-based high entropy $(Ti_{0.2}Zr_{0.2}Hf_{0.2}Nb_{0.2}Ta_{0.2})B_2$–SiC particulate composites, Ceram. Int. 45 (2019) 24508-24514. https://doi.org/10.1016/j.ceramint.2019.08.178

[17] Spark Plasma Sintering: Current Status, New Developments and Challenges. G. Cao, C. Estournés, J. Garay, R.Orrù Eds., published by Elsevier, ISBN: 978-0-12-817744-0 (2019) https://doi.org/10.1016/C2018-0-02428-7

[18] S. Baik, P.F. Becher, Effect of Oxygen contamination on Densification of TiB_2, J. Am. Ceram. Soc. 70: (1987) 527-530. https://doi.org/10.1111/j.1151-2916.1987.tb05699.x

[19] W.G. Fahrenholtz, G.E. Hilmas, S.C. Zhang, S. Zhu, Pressureless Sintering of Zirconium Diboride: Particle Size and Additive Effects, J. Am. Ceram. Soc. 91 (2008) 1398–1404. https://doi.org/10.1111/j.1551-2916.2007.02169.x

[20] S.K. Mishra, L.C. Pathak, Effect of carbon and titanium carbide on sintering behavior of zirconium diboride, J. Alloys Compd. 465 (2008) 547–555. https://doi.org/10.1016/j.jallcom.2007.11.004

[21] V. Zamora, M. Nygren, F. Guiberteau, A.L. Ortiz, Effect of graphite addition on the spark-plasma sinterability of ZrB_2 and ZrB_2–SiC ultra-high-temperature ceramics, Ceram. Int. 40 (2014) 11457-11464. https://doi.org/10.1016/j.ceramint.2014.03.130

[22] H.B. Ma, J. Zou, P. Lu, J.T. Zhu, Z.Q. Fu, F.F. Xu, G.J. Zhang, Oxygen contamination on the surface of ZrB_2 powders and its removal, Scripta Mater. 127 (2017) 160-164. https://doi.org/10.1016/j.scriptamat.2016.09.020

[23] M. Thompson, W.G. Fahrenholtz, G. Hilmas, Effect of Starting Particle Size and Oxygen Content on Densification of ZrB_2, J. Am. Ceram. Soc. 94 (2011) 429–435. https://doi.org/10.1111/j.1551-2916.2010.04114.x

[24] S.H. Jung, H.C. Oh, J.H. Kim, S.C. Choi, S.H. Lee, H.D. Kim, Pretreatment of zirconium diboride powder to improve densification, J. Alloys Compd. 548 (2013) 173-179. https://doi.org/10.1016/j.jallcom.2012.09.038

[25] C. Musa, R. Orrù, D. Sciti, L. Silvestroni, G. Cao, Synthesis, consolidation and characterization of monolithic and SiC whiskers reinforced HfB_2 ceramics, J. Eur. Ceram. Soc.33 (2013) 603-614. https://doi.org/10.1016/j.jeurceramsoc.2012.10.004

[26] R. Licheri, C. Musa, R. Orrù, G. Cao, D. Sciti, L. Silvestroni, Bulk Monolithic Zirconium and Tantalum Diborides by Reactive and Non-reactive Spark Plasma Sintering, J. Alloys Compd 663 (2016) 351-359. https://doi.org/10.1016/j.jallcom.2015.12.096

[27] E. Sani, L. Mercatelli, M. Meucci, A. Balbo, C. Musa, R. Licheri, R. Orrù, G. Cao, Optical properties of dense zirconium and tantalum diborides for solar thermal absorbers, Renew. Energy. 91 (2016) 340-346. https://doi.org/10.1016/j.renene.2016.01.068

[28] A. Cincotti, R. Licheri, A.M. Locci, R. Orrù, G. Cao, A review on combustion synthesis of novel materials: recent experimental and modeling results, J. Chem. Technol. Biotechnol. 78 (2003) 122-127. https://doi.org/10.1002/jctb.757

[29] F.L. Matthews, R. Rawlings Composite Materials: Engineering and Science. Chapman & Hall, Great Britain; 1994. ISBN: 9781855734739

[30] H.O.Pierson Handbook of Carbon, Graphite, Diamonds and Fullerenes. Published by Elsevier; 1994. ISBN 978-0-8155-1339-1

[31] L. Lutterotti, R. Ceccato, R. Dal Maschio, E. Pagani, Quantitative analysis of silicate glass in ceramic materials by the Rietveld method, Mater. Sci. Forum 87 (1998) 278-281. https://doi.org/10.4028/www.scientific.net/MSF.278-281.87

[32] C.A. Schneider, W.S. Rasband, K.W. Eliceiri, NIH Image to ImageJ: 25 years of image analysis, Nat. methods 2012;9(7):671-675. https://doi.org/10.1038/nmeth.2089

[33] C. Musa, R. Licheri, R. Orrù, G. Cao, Synthesis, Sintering, and Oxidative Behavior of HfB_2–$HfSi_2$ Ceramics Ind. Eng. Chem. Res. 53(22) (2014) 9101-9108. https://doi.org/10.1021/ie4032692

[34] E. Sani, M. Meucci, L. Mercatelli, A. Balbo, C. Musa, R. Licheri, R. Orrù, G. Cao, Titanium diboride ceramics for solar thermal absorbers, Sol. Energy Mater Sol. Cells 169 (2017) 313-319. https://doi.org/10.1016/j.solmat.2017.05.038

[35] A.S. Mukasyan, D.O. Moskovskikh, A.A. Nepapushev, J.M. Pauls, S.I. Roslyakov, Ceramics from self-sustained reactions: Recent advances, J. Eur. Ceram. Soc. 40 (2020) 2512–2526. https://doi.org/10.1016/j.jeurceramsoc.2019.12.028

Captions for figures

Figure 1. (a) XRD patterns and related Rietveld profiles of $(Hf_{0.2}Mo_{0.2}Ta_{0.2}Nb_{0.2}Ti_{0.2})B_2$ bulk samples obtained by SPS for all graphite amounts (wt.%) added to the SHS powders. (b) Details of 0, 1 and 10 wt.% C patterns in the 2θ range 20-50°

Figure 2. Mass fractions (a) of different phases detected in $(Hf_{0.2}Mo_{0.2}Ta_{0.2}Nb_{0.2}Ti_{0.2})B_2$ samples obtained by SPS and (b) crystallite size of the HEB phase as a function of the graphite added (wt.%) to the SHS powders.

Figure 3. Effect of graphite addition on the density of the $(Hf_{0.2}Mo_{0.2}Ta_{0.2}Nb_{0.2}Ti_{0.2})B_2$ samples obtained by SPS. The theoretical density values are determined using a rule of mixture, by considering the amount of graphite added to the SHS powders.

Figure 4. Cross sectional SEM micrographs and corresponding EDS elemental maps of the $(Hf_{0.2}Mo_{0.2}Ta_{0.2}Nb_{0.2}Ti_{0.2})B_2$ samples produced by SPS using different graphite amounts: a) 0 wt.%; b) 0.5 wt.%; c) 1 wt.%; d) 3 wt.%; and e) 10 wt.%.

Figure 5 XRD patterns of reactants and related product obtained by SHS for the synthesis of $(Hf_{0.2}Mo_{0.2}Ta_{0.2}Zr_{0.2}Ti_{0.2})B_2$ according to Eq. (2)

Figure 6. (a) XRD patterns and related Rietveld profiles of $(Hf_{0.2}Mo_{0.2}Ta_{0.2}Zr_{0.2}Ti_{0.2})B_2$ bulk samples obtained by SPS for all graphite amounts (wt.%) added to the SHS powders. (b) Details of 0, 1 and 3 wt.% C patterns in the 2θ range 20-50°

Figure 7. Mass fractions (a) of different phases detected in $(Hf_{0.2}Mo_{0.2}Ta_{0.2}Zr_{0.2}Ti_{0.2})B_2$ samples obtained by SPS and (b) crystallite size of the HEB phase as a function of the graphite added (wt.%) to the SHS powders.

Figure 8. Effect of graphite addition on the density of the $(Hf_{0.2}Mo_{0.2}Ta_{0.2}Zr_{0.2}Ti_{0.2})B_2$ samples obtained by SPS. The theoretical density values are determined using a rule of mixture, by considering the amount of graphite added to the SHS powders.

Figure 9. Sample shrinkage curves relative to the fabrication by SPS of $(Hf_{0.2}Mo_{0.2}Ta_{0.2}Zr_{0.2}Ti_{0.2})B_2$ when starting from powder mixtures without and with the addition of graphite (1 and 3 wt.%). The temperature profile is also reported.

Figure 10. Cross sectional SEM micrographs and corresponding EDS elemental maps of the $(Hf_{0.2}Mo_{0.2}Ta_{0.2}Zr_{0.2}Ti_{0.2})B_2$ samples produced by SPS with (a) no graphite and (b) 1 wt.% C.

Figure 1. (a) XRD patterns and related Rietveld profiles of $(Hf_{0.2}Mo_{0.2}Ta_{0.2}Nb_{0.2}Ti_{0.2})B_2$ bulk samples obtained by SPS for all graphite amounts (wt.%) added to the SHS powders. (b) Details of 0, 1 and 10 wt.% C patterns in the 2θ range 20-50°

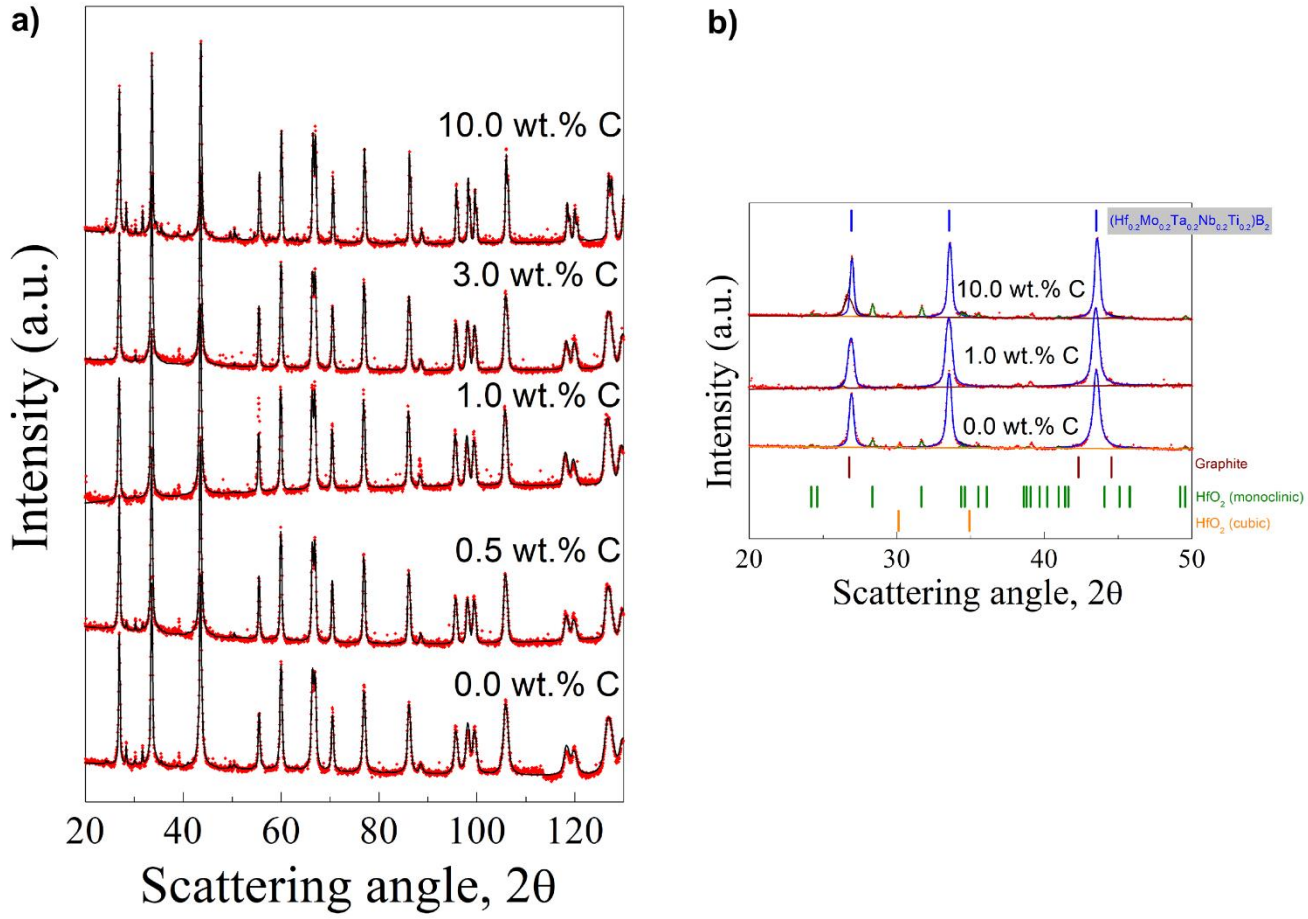

Figure 2. Mass fractions (a) of different phases detected in $(Hf_{0.2}Mo_{0.2}Ta_{0.2}Nb_{0.2}Ti_{0.2})B_2$ samples obtained by SPS and (b) crystallite size of the HEB phase as a function of the graphite added (wt.%) to the SHS powders.

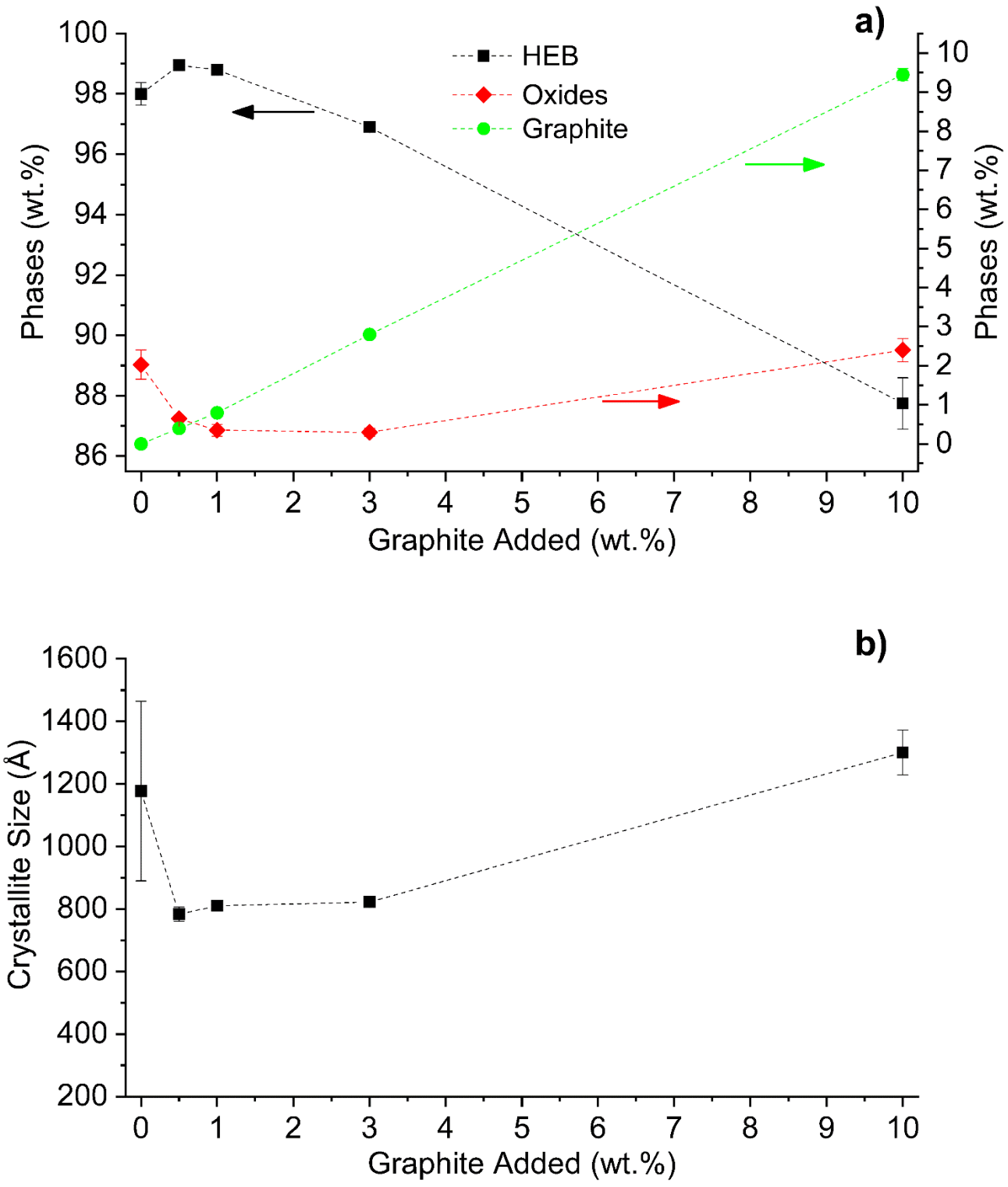

Figure 3. Effect of graphite addition on the density of the $(Hf_{0.2}Mo_{0.2}Ta_{0.2}Nb_{0.2}Ti_{0.2})B_2$ samples obtained by SPS. The theoretical density values are determined using a rule of mixture, by considering the amount of graphite added to the SHS powders.

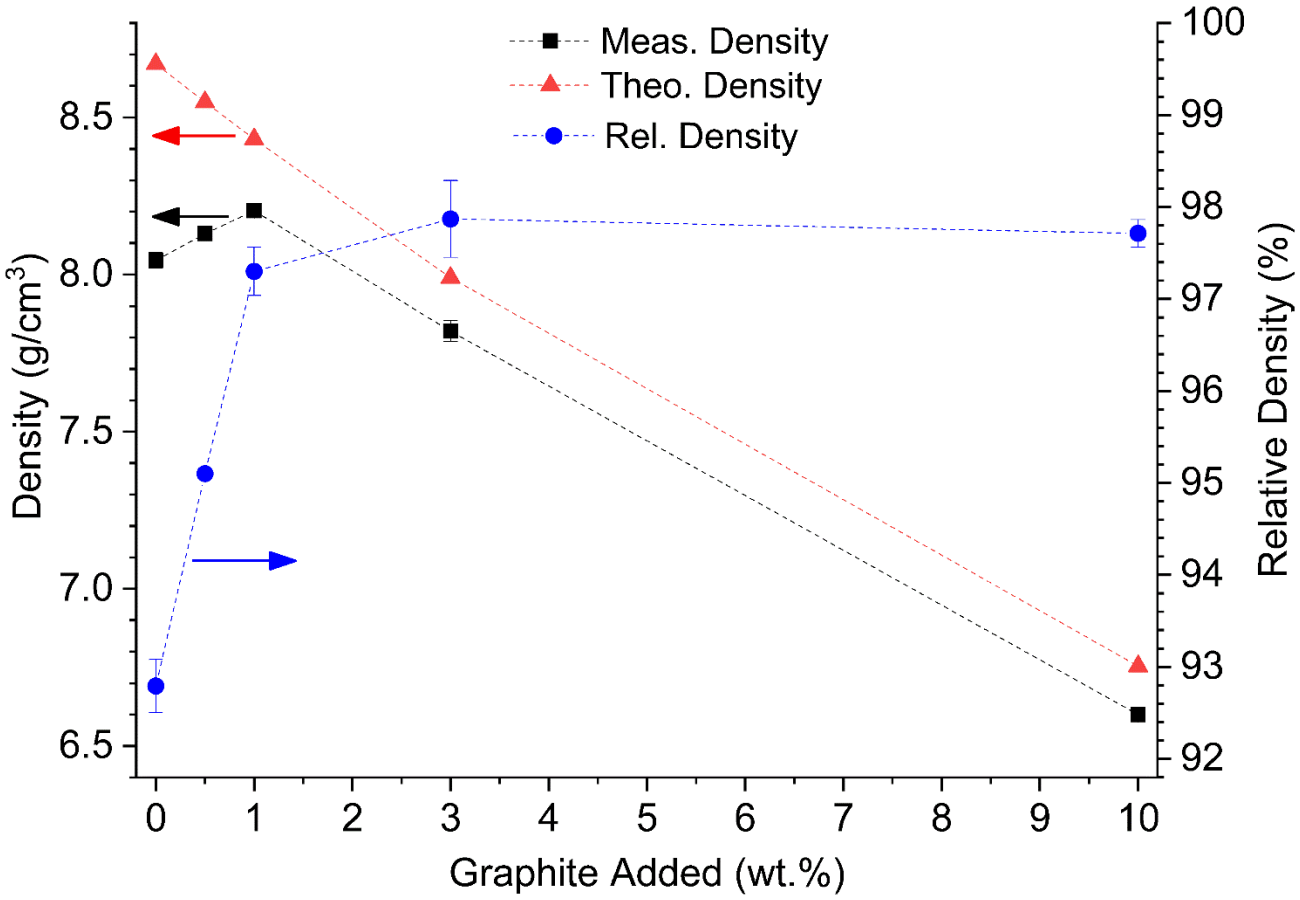

Figure 4. Cross sectional SEM micrographs and corresponding EDS elemental maps of the $(Hf_{0.2}Mo_{0.2}Ta_{0.2}Nb_{0.2}Ti_{0.2})B_2$ samples produced by SPS using different graphite amounts: a) 0 wt.%; b) 0.5 wt.%; c) 1 wt.%; d) 3 wt.%; and e) 10 wt.%.

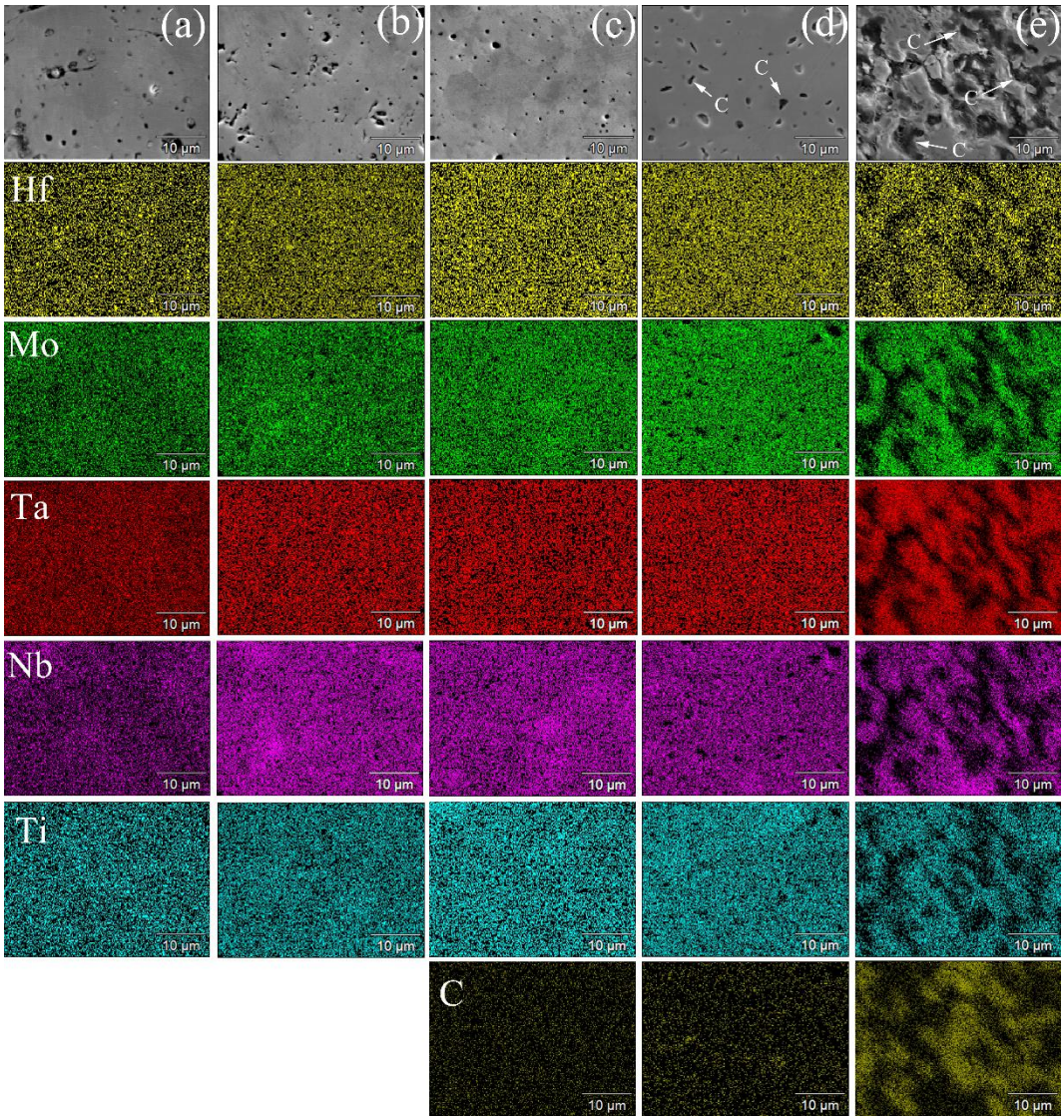

Figure 5 XRD patterns of reactants and related product obtained by SHS for the synthesis of $(Hf_{0.2}Mo_{0.2}Ta_{0.2}Zr_{0.2}Ti_{0.2})B_2$ according to Eq. (2)

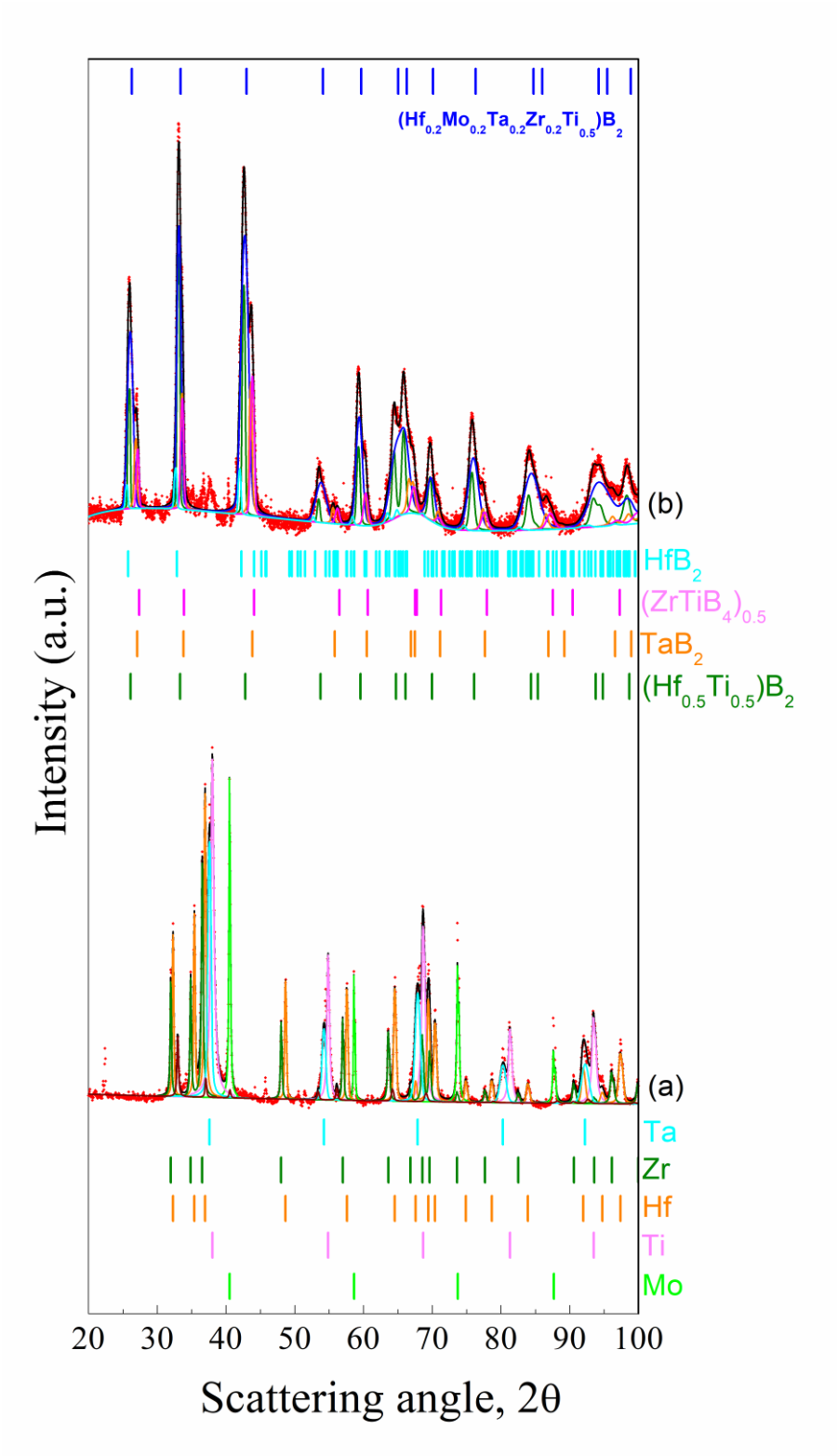

Figure 6. (a) XRD patterns and related Rietveld profiles of $(Hf_{0.2}Mo_{0.2}Ta_{0.2}Zr_{0.2}Ti_{0.2})B_2$ bulk samples obtained by SPS for all graphite amounts (wt.%) added to the SHS powders. (b) Details of 0, 1 and 3 wt.% C patterns in the 2θ range 20-50°

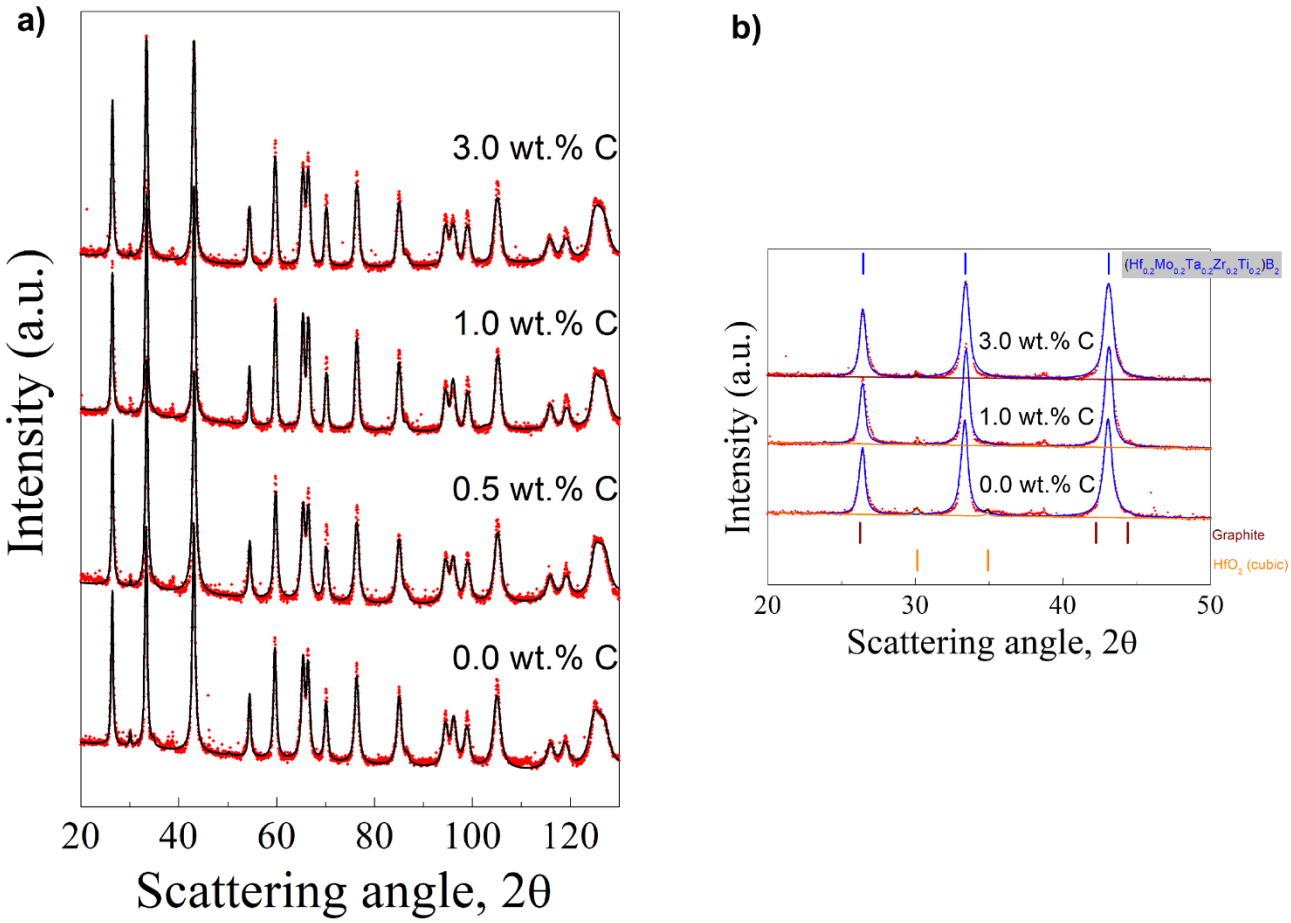

Figure 7. Mass fractions (a) of different phases detected in ($Hf_{0.2}Mo_{0.2}Ta_{0.2}Zr_{0.2}Ti_{0.2}$)$B_2$ samples obtained by SPS and (b) crystallite size of the HEB phase as a function of the graphite added (wt.%) to the SHS powders.

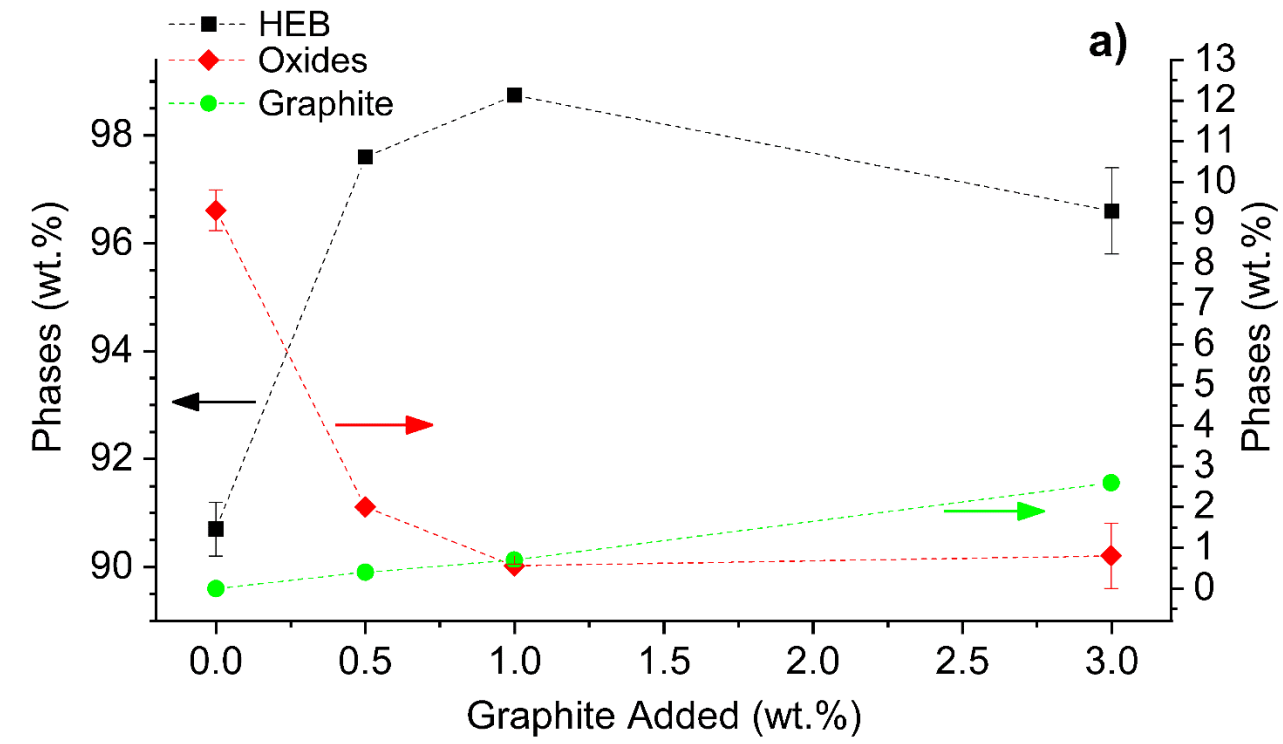

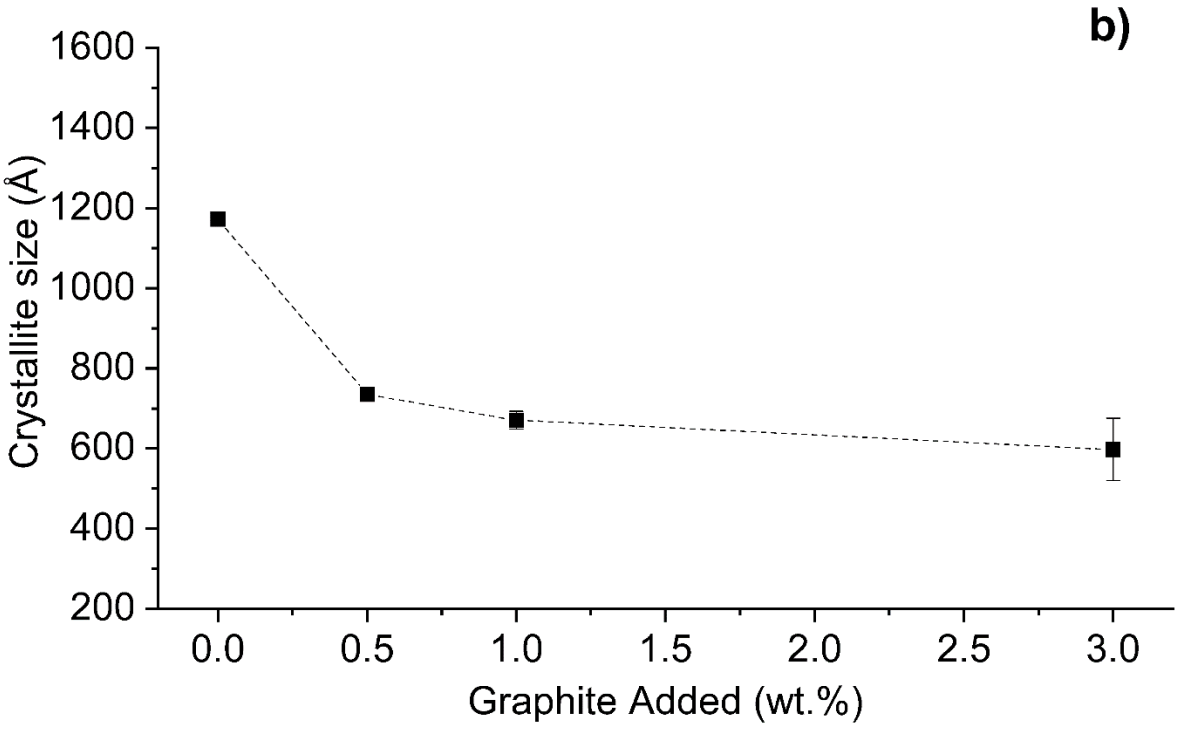

Figure 8. Effect of graphite addition on the density of the $(Hf_{0.2}Mo_{0.2}Ta_{0.2}Zr_{0.2}Ti_{0.2})B_2$ samples obtained by SPS. The theoretical density values are determined using a rule of mixture, by considering the amount of graphite added to the SHS powders.

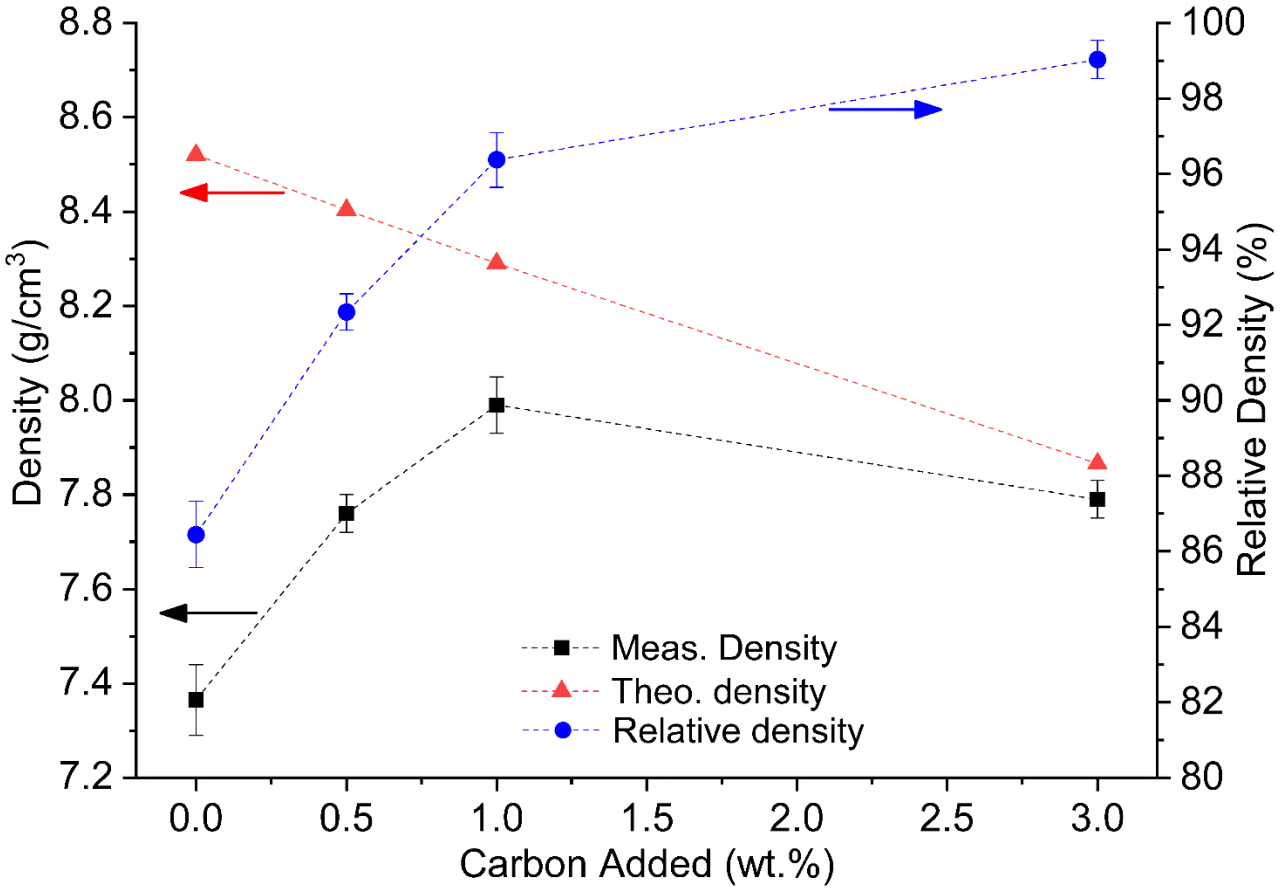

Figure 9. Sample shrinkage curves relative to the fabrication by SPS of $(Hf_{0.2}Mo_{0.2}Ta_{0.2}Zr_{0.2}Ti_{0.2})B_2$ when starting from powder mixtures without and with the addition of graphite (1 and 3 wt.%). The temperature profile is also reported.

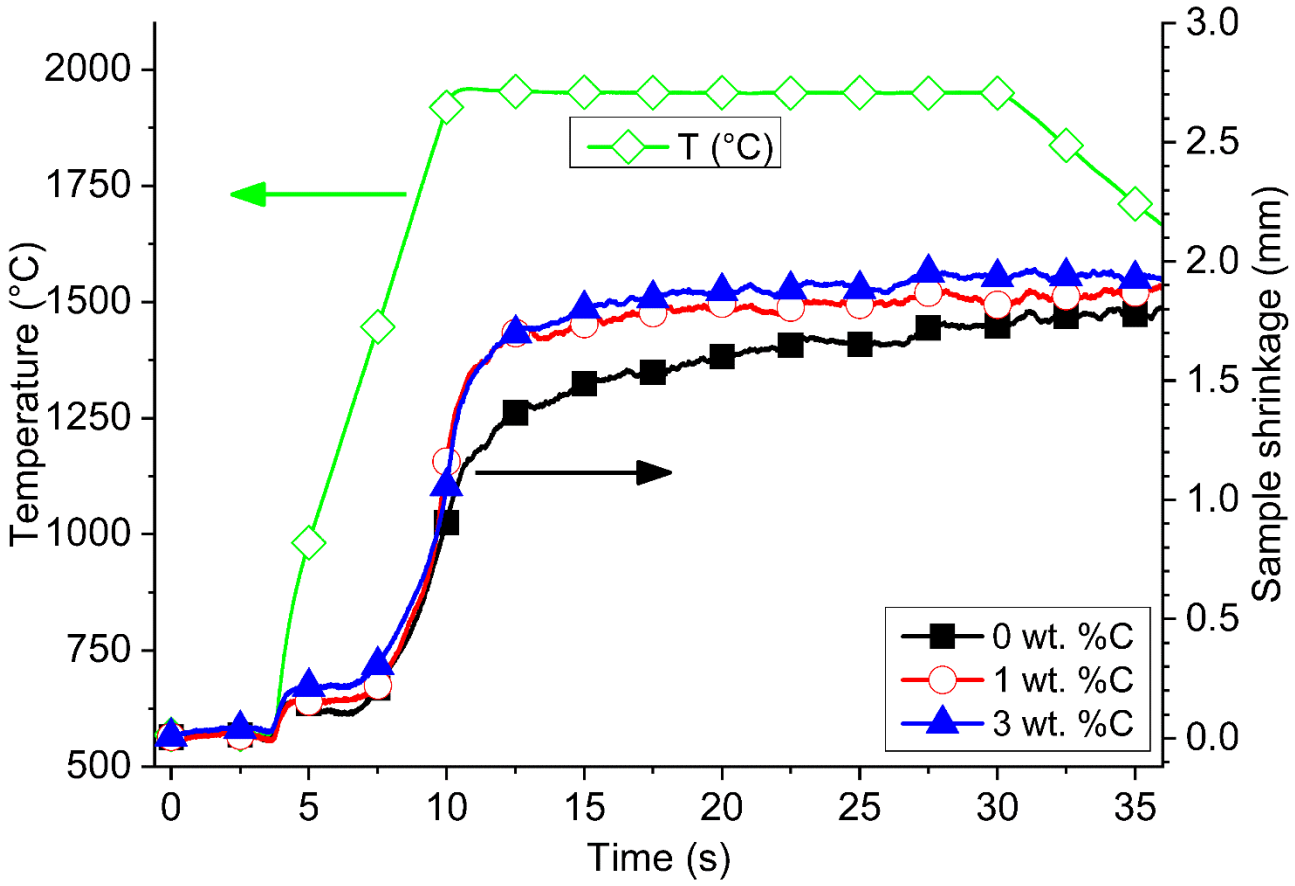

Figure 10. Cross sectional SEM micrographs and corresponding EDS elemental maps of the $(Hf_{0.2}Mo_{0.2}Ta_{0.2}Zr_{0.2}Ti_{0.2})B_2$ samples produced by SPS with (a) no graphite and (b) 1 wt.% C.